



# Structures and properties of 1,8,15,22-tetrasubstituted phthalocyaninato zinc and nickel complexes: Substitution and axially coordination effects study based on density functional theory calculations

Liang Wan, Yuxing Zhang\*, Dongdong Qi, Jianzhuang Jiang

Department of Chemistry, University of Science and Technology Beijing, Beijing 100083, China

## ARTICLE INFO

### Article history:

Received 30 December 2009  
Received in revised form 3 March 2010  
Accepted 9 March 2010  
Available online 16 March 2010

### Keywords:

Phthalocyanine  
Substitution effect  
IR spectra  
Electronic absorption spectra  
Density functional theory

## ABSTRACT

On the basis of the density functional theory (DFT) calculation of ZnPc (**1**), Zn[Pc( $\alpha$ -OC<sub>5</sub>H<sub>11</sub>)<sub>4</sub>] (**2**), Ni[Pc( $\alpha$ -OC<sub>5</sub>H<sub>11</sub>)<sub>4</sub>] (**3**), and Zn[Pc( $\alpha$ -OC<sub>5</sub>H<sub>11</sub>)<sub>4</sub>] $\cdot$ H<sub>2</sub>O (**4**), the effects of non-peripheral substitution, different transition metals, and axial water coordination on the molecular structure, molecular orbital, atomic charge, infrared (IR) spectrum, and electronic absorption spectrum were investigated. The calculation results reveal that bulky 3-pentyloxy groups at the non-peripheral positions of the phthalocyanine ring evince great changes in structure and properties: they deflect the isoindole units, lift the frontier molecular orbitals, alter the atomic charge distribution, shift the bands of IR and electronic absorption spectra, etc. Though the central metal can shorten or lengthen the bond length, its effect on the electronic structure and properties of the phthalocyanine complex is very limited. Axial coordination significantly enhances the non-planarity of the phthalocyanine ring and, thus, alters the electronic structure, which is important for the formation of novel dimeric supramolecular structures through intermolecular hydrogen bonds. In addition, the calculated structures of **3** as well as the simulated IR and electronic absorption spectra of **4** were compared with the experimental data and showed good agreement.

© 2010 Elsevier Inc. All rights reserved.

## 1. Introduction

Phthalocyanines have been important dyes and pigments since their synthesis at the beginning of last century [1–3]. In recent years, phthalocyanine derivatives have been applied as charge carriers for photocopiers and laser printers as well as materials for optical storage [4–7]. Due to their high thermal and chemical stability, many potential applications are expected, such as oxidation catalysts [8], solar cell functional materials [9,10], gas sensors [11,12], nonlinear optical limiting devices [13–15], photodynamic therapy agents [16–18], antimycotic materials [19], and corrosion inhibitors [20].

Phthalocyanine can coordinate with almost all the metals in the Periodic Table, and these phthalocyaninato metal complexes vary greatly in their structures and properties. In addition, peripheral substitution, non-peripheral substitution, and axial coordination can also significantly affect the structure and properties of phthalocyanine compounds. Many studies have been carried out to demonstrate the effect of these factors. For example, Langford et al. studied the photoelectrochemistry and spectroscopy of films formed by phthalocyaninato metal complexes including MgPc,

FePc, NiPc, and ZnPc on a transparent semiconducting electrode in 1980 [21]. The influence of alkyl substituent chain length, peripheral versus non-peripheral substitution positions, and coordinated central metal (2H, Cu<sup>2+</sup>, Ni<sup>2+</sup>, Zn<sup>2+</sup> and Cl–Al<sup>3+</sup>) on the mesophase behavior and spectroscopic properties of the phthalocyanine compounds was described by Langner et al. in 2006 [22]. In 2007, Lo et al. studied the effect of peripheral chlorine substitution on the photophysical and photodynamic properties of highly photocytotoxic glucosylated silicon (**IV**) phthalocyanines [23]. Despite the wide experimental studies, theoretical investigation at the DFT level has been scarce, especially for systematical studies considering the influence of all the three factors including different central metals, peripheral or non-peripheral substituents, and axial ligands on the structure and properties of the phthalocyanine complex.

With the development of the computer industry and calculation methods, calculation and simulation of large molecules have been possible. The density functional theory (DFT) method, which includes electron correlation effects, has proved suitable for calculating the energy-minimized structure of H<sub>2</sub>Pc and its metal derivatives [24–31]. Russo et al. discussed whether phthalocyanines and their substituted  $\alpha$ -para-(methoxy)phenyl derivatives can act as photosensitizers in photodynamic therapy with TDDFT study in 2009 [18]. This group comparatively studied the structures and properties of PbPc, SnPc, PcSnCl<sub>2</sub>, GePc, and PcGeCl<sub>2</sub> [24]

\* Corresponding author. Tel.: +86 10 6233 4509; fax: +86 10 6233 2462.

E-mail addresses: [yxzhang@ustb.edu.cn](mailto:yxzhang@ustb.edu.cn), [zhangyuxing@sdu.edu.cn](mailto:zhangyuxing@sdu.edu.cn) (Y. Zhang).

**Table 1**Calculated main structural parameters of ZnPc (**1**), Zn[Pc( $\alpha$ -OC<sub>5</sub>H<sub>11</sub>)<sub>4</sub>] (**2**), Ni[Pc( $\alpha$ -OC<sub>5</sub>H<sub>11</sub>)<sub>4</sub>] (**3**), and Zn[Pc( $\alpha$ -OC<sub>5</sub>H<sub>11</sub>)<sub>4</sub>] $\cdot$ H<sub>2</sub>O (**4**).

Parameter <sup>a</sup>	<b>1</b>	<b>2</b>	<b>3</b>	<b>4</b>			
				Isoindole-1	Isoindole-2	Isoindole-3	Isoindole-4
M–N <sub>1</sub>	2.01	2.02	1.93	2.05	2.04	2.04	2.05
N <sub>1</sub> –C <sub><math>\alpha</math>1</sub>	1.37	1.38	1.38	1.37	1.37	1.37	1.37
N <sub>1</sub> –C <sub><math>\alpha</math>2</sub>	1.37	1.37	1.37	1.37	1.37	1.37	1.37
C <sub><math>\alpha</math>1</sub> –N <sub>2</sub>	1.33	1.33	1.32	1.33	1.33	1.33	1.33
C <sub><math>\alpha</math>2</sub> –N <sub>2</sub>	1.33	1.33	1.32	1.33	1.33	1.33	1.33
C <sub><math>\alpha</math>1</sub> –C <sub><math>\beta</math>1</sub>	1.46	1.46	1.46	1.46	1.47	1.47	1.46
C <sub><math>\alpha</math>2</sub> –C <sub><math>\beta</math>2</sub>	1.46	1.46	1.45	1.46	1.46	1.46	1.46
C <sub><math>\beta</math>1</sub> –C <sub><math>\gamma</math>1</sub>	1.40	1.41	1.41	1.41	1.41	1.41	1.41
C <sub><math>\beta</math>2</sub> –C <sub><math>\gamma</math>2</sub>	1.40	1.39	1.39	1.39	1.39	1.39	1.39
C <sub><math>\beta</math>1</sub> –C <sub><math>\beta</math>2</sub>	1.41	1.41	1.40	1.41	1.41	1.41	1.41
C <sub><math>\gamma</math>1</sub> –C <sub><math>\delta</math>1</sub>	1.40	1.40	1.40	1.40	1.40	1.40	1.40
C <sub><math>\gamma</math>2</sub> –C <sub><math>\delta</math>2</sub>	1.40	1.39	1.39	1.39	1.39	1.39	1.39
C <sub><math>\delta</math>1</sub> –C <sub><math>\delta</math>2</sub>	1.41	1.41	1.41	1.41	1.40	1.40	1.41
N <sub>1</sub> –M–N <sub>1</sub>	90	90	90	88	89	88	88
C <sub><math>\alpha</math>1</sub> –N <sub>1</sub> –C <sub><math>\alpha</math>2</sub>	110	110	107	110	110	110	110
N <sub>1</sub> –C <sub><math>\alpha</math>1</sub> –C <sub><math>\beta</math>1</sub>	108	108	110	108	108	108	108
N <sub>1</sub> –C <sub><math>\alpha</math>2</sub> –C <sub><math>\beta</math>2</sub>	108	108	110	109	109	109	109
C <sub><math>\alpha</math>1</sub> –N <sub>2</sub> –C <sub><math>\alpha</math>2</sub>	125	125	122	125	125	125	125
C <sub><math>\gamma</math>1</sub> –O		1.35	1.35	1.36	1.36	1.36	1.36
O–C <sub>1</sub>		1.44	1.44	1.44	1.44	1.44	1.44
C <sub>1</sub> –C <sub>2</sub>		1.53	1.54	1.53	1.53	1.53	1.53
C <sub>2</sub> –C <sub>3</sub>		1.53	1.53	1.53	1.53	1.53	1.53
C <sub>1</sub> –C <sub>4</sub>		1.54	1.53	1.54	1.54	1.54	1.54
C <sub>4</sub> –C <sub>5</sub>		1.53	1.53	1.53	1.53	1.53	1.53
C <sub><math>\gamma</math>1</sub> –O–C <sub>1</sub>		122	122	122	122	122	122
C <sub>2</sub> –C <sub>1</sub> –C <sub>4</sub>		114	114	114	114	114	114

<sup>a</sup> See Fig. 1 for atomic labeling.

and investigated the effects of non-peripheral [25] and peripheral substituents [26] on the structure and properties of PbPc.

In 2008, a novel dimeric supramolecular structure, {Zn[Pc( $\alpha$ -OC<sub>5</sub>H<sub>11</sub>)<sub>4</sub>] $\cdot$ H<sub>2</sub>O}<sub>2</sub>, formed by two molecules of 1,8,15,22-tetrakis(3-pentyloxy)-phthalocyaninato zinc complex Zn[Pc( $\alpha$ -OC<sub>5</sub>H<sub>11</sub>)<sub>4</sub>] was revealed by X-ray single crystal analysis in our group [32]. However, from ZnPc to Zn[Pc( $\alpha$ -OC<sub>5</sub>H<sub>11</sub>)<sub>4</sub>] $\cdot$ H<sub>2</sub>O, the change of structure and properties by axial water coordination and non-peripheral (3-pentyloxy) substitution is still not clear. In addition, the spectroscopic properties of Zn[Pc( $\alpha$ -OC<sub>5</sub>H<sub>11</sub>)<sub>4</sub>] $\cdot$ H<sub>2</sub>O have not yet been clearly described. As the first example of a supramolecular structure formed from phthalocyanine complexes with transition metals via H<sub>2</sub>O-involved hydrogen bonding interaction, clarifying the significant function of axial coordination associated with non-peripheral substitution on the electronic structure and aggregation behavior of phthalocyanine compounds will be helpful in designing new functional materials of phthalocyanine.

In this paper, we comparatively studied the molecular structure, molecular orbitals, atomic charge, and IR and electronic absorption spectra of ZnPc (**1**), Zn[Pc( $\alpha$ -OC<sub>5</sub>H<sub>11</sub>)<sub>4</sub>] (**2**), Ni[Pc( $\alpha$ -OC<sub>5</sub>H<sub>11</sub>)<sub>4</sub>] (**3**), and Zn[Pc( $\alpha$ -OC<sub>5</sub>H<sub>11</sub>)<sub>4</sub>] $\cdot$ H<sub>2</sub>O (**4**) in detail with the DFT method. The effects of non-peripheral substitution with 3-pentyloxy groups, transition metals as well as axial coordination with water molecules on the molecular structure and properties of phthalocyaninato zinc complex are also described.

## 2. Computational details

The primal input structure of **1** was obtained by putting Zn<sup>2+</sup> ions into the central cavity of the phthalocyanine dianion, and 3-pentyloxy groups were added at the non-peripheral  $\alpha$  position of the optimized structure of ZnPc to construct molecule **2**. One water molecule was further introduced at the axial position of **2**, forming the primal structure of **4**. The primal structure of **3** was obtained by directly changing a zinc ion of **2** to a nickel ion. The hybrid density functional B3LYP (Becke–Lee–Young–Parr composite of exchange–correlation functional) method [33] was used for both geometry

optimization and property calculations. In all work, the LANL2DZ basis set [34–37] was used for the central metal atoms, and the 6-31G(d) basis set was used for the other atoms (basis set **I**).

The effects of basis set convergence were examined by adding diffuse functions to the basis set [6-31+G(d) for C, H and N atoms, LANL2DZ basis set for Zn] (**II**), and by using a larger triple zeta basis set [6-311+G(d) for C, H and N atoms, LANL2DZ basis set for Zn] (**III**) and calculating the structure and properties of ZnPc as an example using these basis sets. The calculation results revealed that the effects of basis set were rather small. In detail, comparing levels **I** and **II**, the largest difference between the bond lengths of the two levels is only 0.026 Å for Zn–N bond with the biggest relative error of merely 0.8% for C <sub>$\alpha$</sub> –N<sub>2</sub>–C <sub>$\alpha$</sub>  bond angle. As for **I** and **III**, the biggest difference comes from the same bond and angle with the relative errors about 1.3% and 0.8% respectively. The energy gap between HOMO and LUMO was revealed to be 2.18 eV, 2.15 eV and 2.14 eV for ZnPc on the **I**, **II** and **III** levels respectively. The biggest difference of the gap energy is only 0.04 eV, indicating the good correspondence for the orbital energy gap obtained on the three levels. As a total result, basis set **I** is accurate enough for calculating both the geometry and electronic structure of phthalocyanine complexes. For the purpose of time economy efficiency, calculations are therefore performed at the B3LYP/[6-31G(d) for C, H and N atoms, LANL2DZ basis set for Zn] level in the present work. In addition, due to the fact that the Kohn–Sham molecular orbitals can afford a direct connection with the LCAO–MO treatments based on semiempirical or Hartree–Fock orbitals, while at the same time having the benefit of the high accuracy of DFT treatment of the excitation energies [27], DFT method shows enough validity and relevance in calculating the electronic structure as well as HOMO–LUMO gap of phthalocyanine complexes.

The Berny algorithm using redundant internal coordinates [38] was employed in the energy-minimization process, and the default convergence criterion was used throughout. Using the energy-minimized structure generated in the previous step, normal coordinate analysis was carried out, and the primarily calculated vibration frequency was scaled by a factor of 0.9614 [39]. Later, the

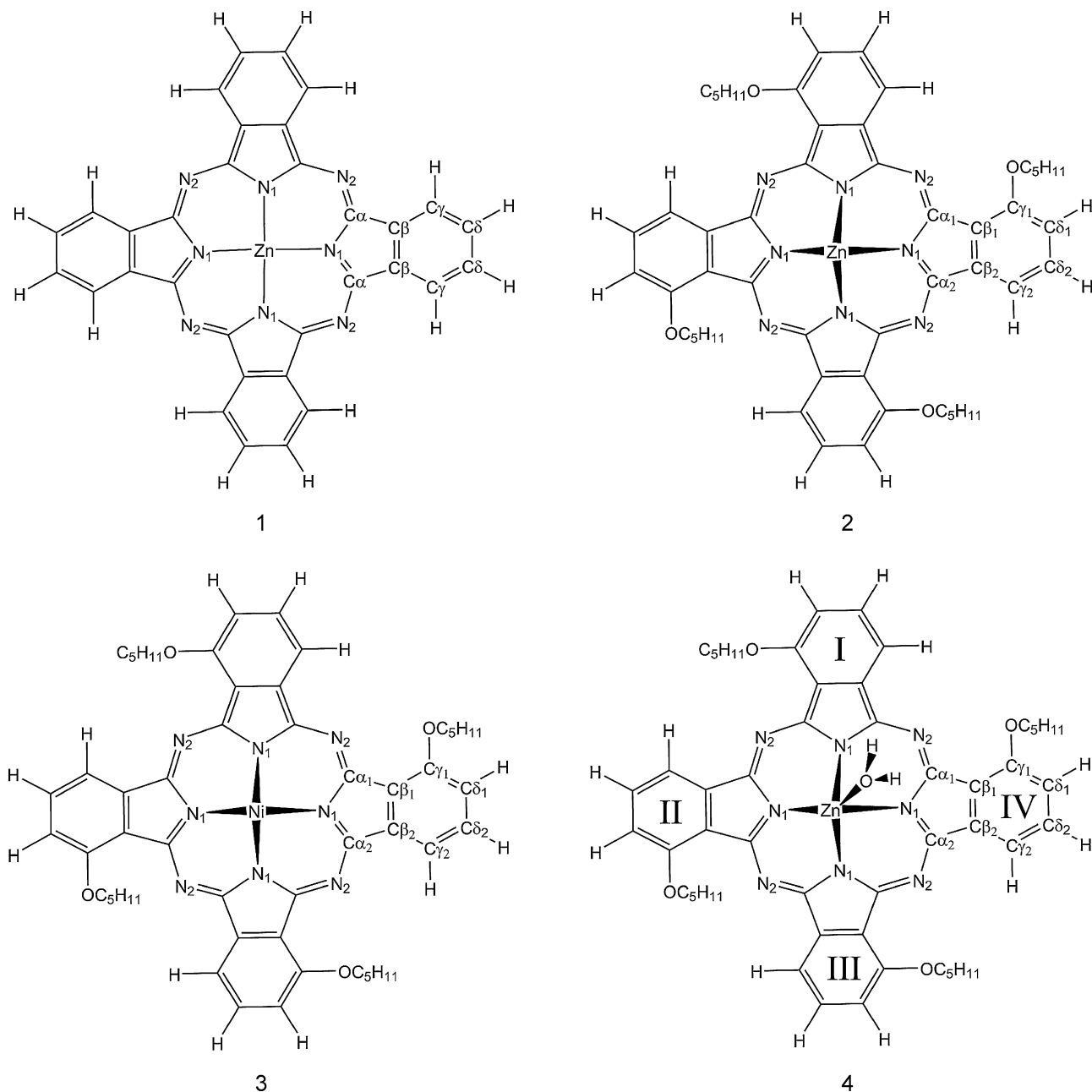


Fig. 1. Schematic molecular structures and atomic labels of ZnPc (**1**), Zn[Pc( $\alpha$ -OC<sub>5</sub>H<sub>11</sub>)<sub>4</sub>] (**2**), Ni[Pc( $\alpha$ -OC<sub>5</sub>H<sub>11</sub>)<sub>4</sub>] (**3**), and Zn[Pc( $\alpha$ -OC<sub>5</sub>H<sub>11</sub>)<sub>4</sub>]-H<sub>2</sub>O (**4**).

charge distribution was calculated using a full natural bond orbital analysis (NBO) population method [40] with the NBO 3.1 software in the Gaussian 03 program [41]. The electronic absorption spectra were calculated using the TD-DFT method based on the optimized structures with forty singlet-excited states. Gaussian bands with half-bandwidths of 500 cm<sup>-1</sup> were used to simulate the electronic absorption spectra. All the calculations were carried out using the Gaussian 03 program [41].

### 3. Results and discussion

#### 3.1. Molecular structure

The structure and atom labeling of **1–4** are shown in Fig. 1, and the main structural parameters of **1–4** taken from the calculation results are listed in Table 1. The energy-minimized geometry has *D*<sub>4h</sub> symmetry for **1**, *C*<sub>4</sub> for **2** and **3**, and *C*<sub>1</sub> for **4**. No

imaginary vibration was found in the following frequency calculations of the four complexes, indicating that the energy-minimized structures of the four complexes are at the true energy minimum.

Table 2 compares the calculated structural parameter of **3** with the X-ray crystallography data. The differences between the experimental and calculated structures are shown in Fig. 2. As can be seen, the largest difference in bond length is only 0.05 Å for C<sub>2</sub>–C<sub>3</sub>, indicating that the results obtained from the DFT method with the B3LYP functional correspond well with the experimental ones. As for the main bond angle shown in Table 2 and Fig. 2, the greatest difference comes from C<sub>2</sub>–C<sub>1</sub>–C<sub>4</sub>, with a departure of 1.4°, followed by C<sub>α1</sub>–N<sub>1</sub>–C<sub>α2</sub> with 0.9°. The good agreement indicates that our calculation method is reliable for simulating large molecules with more than 120 atoms. The good consistency between experiments and calculations of **1** and **4** is shown in Tables S1 and S2 (Supplementary Data). It is worth noting that the largest difference for

**Table 2**  
Experimental and calculated main structural parameters of Ni[Pc( $\alpha$ -OC<sub>5</sub>H<sub>11</sub>)<sub>4</sub>] (**3**).

Parameter <sup>a</sup>	Calculated	Experimental
Ni–N <sub>1</sub>	1.92	1.90
N <sub>1</sub> –C <sub><math>\alpha</math>1</sub>	1.38	1.38
Ni–C <sub><math>\alpha</math>2</sub>	1.37	1.37
C <sub><math>\alpha</math>1</sub> –N <sub>2</sub>	1.32	1.32
C <sub><math>\alpha</math>2</sub> –N <sub>2</sub>	1.32	1.32
C <sub><math>\alpha</math>1</sub> –C <sub><math>\beta</math>1</sub>	1.46	1.44
C <sub><math>\alpha</math>2</sub> –C <sub><math>\beta</math>2</sub>	1.45	1.45
C <sub><math>\beta</math>1</sub> –C <sub><math>\gamma</math>1</sub>	1.41	1.40
C <sub><math>\beta</math>2</sub> –C <sub><math>\gamma</math>2</sub>	1.40	1.38
C <sub><math>\beta</math>1</sub> –C <sub><math>\delta</math>1</sub>	1.40	1.39
C <sub><math>\gamma</math>1</sub> –C <sub><math>\delta</math>1</sub>	1.40	1.38
C <sub><math>\gamma</math>2</sub> –C <sub><math>\delta</math>2</sub>	1.39	1.37
C <sub><math>\delta</math>1</sub> –C <sub><math>\delta</math>2</sub>	1.41	1.39
C <sub><math>\gamma</math>1</sub> –O	1.35	1.35
O–C <sub>1</sub>	1.44	1.44
C <sub>1</sub> –C <sub>2</sub>	1.54	1.52
C <sub>2</sub> –C <sub>3</sub>	1.53	1.48
C <sub>1</sub> –C <sub>4</sub>	1.53	1.50
C <sub>4</sub> –C <sub>5</sub>	1.53	1.50
N <sub>1</sub> –Ni–N <sub>1</sub>	90	90
C <sub><math>\alpha</math>1</sub> –N <sub>1</sub> –C <sub><math>\alpha</math>2</sub>	107	107
N <sub>1</sub> –C <sub><math>\alpha</math>1</sub> –C <sub><math>\beta</math>1</sub>	110	110
N <sub>1</sub> –C <sub><math>\alpha</math>2</sub> –C <sub><math>\beta</math>2</sub>	110	111
C <sub><math>\alpha</math>1</sub> –N <sub>2</sub> –C <sub><math>\alpha</math>2</sub>	122	121
C <sub><math>\gamma</math>1</sub> –O–C <sub>1</sub>	122	121
C <sub>2</sub> –C <sub>1</sub> –C <sub>4</sub>	114	113

<sup>a</sup> See Fig. 1 for atomic labeling.

either bond length or bond angle in **3** is on the substituents, while the difference is much smaller for the phthalocyanine macrocycle. This result is attributed to the relatively free extension of the 3-pentyloxy groups of **3**, whose structure is optimized and calculated in a vacuum instead of in the real crystal environment, in which intermolecular interaction significantly limits the extension of substituents.

The introduction of 3-pentyloxy groups makes the molecular symmetry decrease from  $D_{4h}$  for **1** to  $C_4$  for **2** and **3**, which is similar to the previous result [25]. Also in line with the previous findings [25], 3-pentyloxy substitution makes the atoms at the substituted side of isoindole unit farther from the central zinc atom than those at the other side. For example, C <sub>$\beta$ 1</sub>–C <sub>$\gamma$ 1</sub> is about 0.02 Å longer than C <sub>$\beta$ 2</sub>–C <sub>$\gamma$ 2</sub>. The Zn–N distance for **2** was found to increase by about

0.01 Å in comparison with that of **1**, indicating an increased hole radius due to the introduction of 3-pentyloxy groups. The repulsion effect between the beta hydrogen atom at the peripheral position (C <sub>$\delta$ 1</sub>) of the Pc ring and the hydrogen atom of the methenyl atom (C<sub>1</sub>) in **2** makes the 3-pentyloxy groups no longer perpendicular to the Pc plane in **2**, inducing a deviation of C <sub>$\delta$ 1</sub> and C <sub>$\gamma$ 1</sub> atoms from the Pc plane, in contrast to the case in **1**, in which the zinc ion is at the plane formed by the four isoindole nitrogen atoms. As a result, the other atoms on the phthalocyanine macrocycle and the central zinc ion also deviate from the phthalocyanine plane. As shown in Fig. 1 and Table 1, **2** forms a dish-like structure with the zinc atom deviating 0.008 Å away from the plane formed by the four isoindole nitrogen atoms. However, the non-planarity of **2** due to the effect of substituents is much smaller than that of PbPc( $\alpha$ -OC<sub>5</sub>H<sub>11</sub>)<sub>4</sub>, which is probably due to the very large central metal radius [25]. This indicates that the non-planarity caused by the bulky substituents is negligible for planar phthalocyanines if a suitable central metal is chosen.

Replacing the central zinc ion of **2** with nickel, which has smaller ionic radius, also induces changes in the molecular structure. Along with the decrease of the ionic radius, the bond length of M–N<sub>1</sub>, C <sub>$\alpha$ 1</sub>–N<sub>2</sub> (C <sub>$\alpha$ 2</sub>–N<sub>2</sub>), C <sub>$\alpha$ 2</sub>–C <sub>$\beta$ 2</sub> (C <sub>$\alpha$ 1</sub>–C <sub>$\beta$ 1</sub>), and C <sub>$\gamma$ 2</sub>–C <sub>$\delta$ 2</sub> (C <sub>$\gamma$ 1</sub>–C <sub>$\delta$ 1</sub>) decreases from 2.02, 1.33 (1.33), 1.46 (1.46), and 1.39 (1.40) Å for **2** to 1.93, 1.32 (1.32), 1.45 (1.46), and 1.39 (1.40) Å for **3**. In contrast, the bond lengths of N<sub>1</sub>–C <sub>$\alpha$ 1</sub> (N<sub>1</sub>–C <sub>$\alpha$ 2</sub>) and C <sub>$\beta$ 1</sub>–C <sub>$\gamma$ 1</sub> (C <sub>$\beta$ 2</sub>–C <sub>$\gamma$ 2</sub>) for **2** increase to 1.38 (1.37) and 1.41 (1.39) Å in **3**. These results indicate that the replacement can reduce the M–N bond length and shorten or lengthen the bonds on the isoindole ring of the phthalocyanine macrocycle. In addition, the change extent for the bonds of isoindole on the same side of 3-pentyloxy groups is smaller than that on the unsubstituted side, indicating that the steric hindrance of the alkoxy substituent limits the change of bond length in the isoindole ring, especially for those on the substituted side. Furthermore, the change is also found to decrease from bonds near the metal center to the periphery of the phthalocyanine ring, revealing the decreased effect of the central metal substitution from the center to periphery. Similar to **2**, molecule **3** also takes a dish-like structure due to the repulsion effect. However, the non-planarity of **3** is even smaller than that of **2**. The central nickel ion sits only about  $1.4 \times 10^{-5}$  Å above the isoindole nitrogen plane and is 0.02 Å above the plane formed by the four C <sub>$\delta$ 2</sub> atoms.

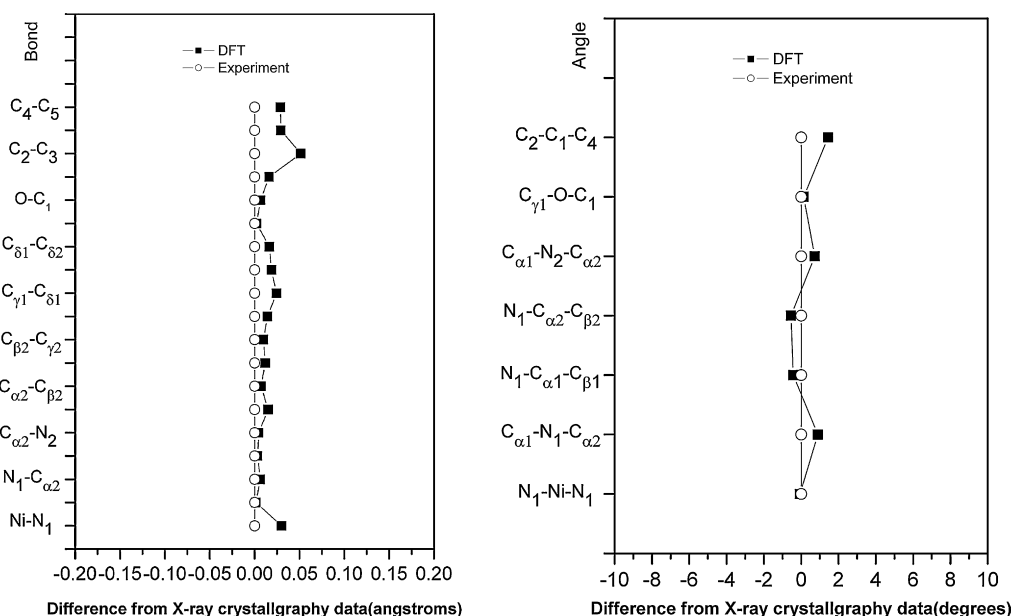


**Fig. 2.** Comparison of main calculated bond lengths and bond angles with the X-ray crystallography data for Ni[Pc( $\alpha$ -OC<sub>5</sub>H<sub>11</sub>)<sub>4</sub>] (**3**).

To clarify the influence of the axial coordination on the structure and properties of phthalocyaninato metal complexes, one water molecule was added at the axial position of **2**, forming the molecule **4**. The calculated structural parameters of **4** are shown in Table 1. As can be seen, the central metal Zn is further pulled out of the molecular plane by the strong attraction of the oxygen atom. At the same time, the isoindole N atoms are drawn off the primary plane of the Pc ring due to the restriction of the Zn–N bond length. It is also true for the other atoms on the phthalocyanine macrocycle. Consequently, the non-planarity of the phthalocyanine complex **4** significantly increases compared with **2**. For example, the distance between Zn and the mean plane formed by the four isoindole nitrogen atoms reaches 0.36 Å for **4**. Because zinc can only coordinate with one of the two lone pair electrons of the oxygen atom, the water molecule makes a tilt angle of about 24.8° relative to the mean plane formed by the four isoindole nitrogen atoms of the phthalocyanine ligand, which not only reduces the molecular symmetry from  $C_4$  for **2** to  $C_1$  for **4** but also induces the structural deformation of the phthalocyanine ring due to the interaction between hydrogen atoms of water and the isoindole nitrogen atoms. The oxygen atom in the water molecule is nearer to the two isoindole nitrogen atoms at the same side of water hydrogen atoms (**I** and **IV**) than to the other isoindole nitrogen atoms (**II** and **III**) (3.21 versus 3.38 Å, Fig. 1 and Table 1). Accordingly, the distance between the  $C_8$  atoms of the two isoindole ring at the same side of the water hydrogen atoms (**I** and **IV**) and the mean plane formed by the four isoindole nitrogen atoms are larger than that between the  $C_8$  atoms of the other two isoindole rings (**II** and **III**). Despite the increased central ion deviation from the plane and the larger structural deformation in **4** than in **2**, the difference between the structural parameters of the phthalocyanine ring for **4** and **2** is not large, with the greatest difference only 0.002 Å for the  $N_1-C_{\alpha 1}$  bond. It is worth pointing out that, due to the large distance between one hydrogen atom of water and the nearest isoindole nitrogen atom (2.99 Å) and the unsuited orientation in **4**, there is no intramolecular hydrogen bond. However, the two hydrogen atoms of the water molecule may form two hydrogen bonds with the electron-abundant oxygen and nitrogen atom from another molecule of **4**, which, in fact, has been proven true by single crystal X-ray structure analysis [32]. In addition, though very slight, the non-planarity of molecule **2** is very important for the two **2** molecules to form the dimeric supramolecular structure via the  $H_2O$ -involved hydrogen bonding interaction instead of forming a one-dimensional chain by coordinating two  $H_2O$  molecules, as in the 5,15-Di[4-(5-acetylsulfanyl)pentoxy]phenyl]porphyrin zinc

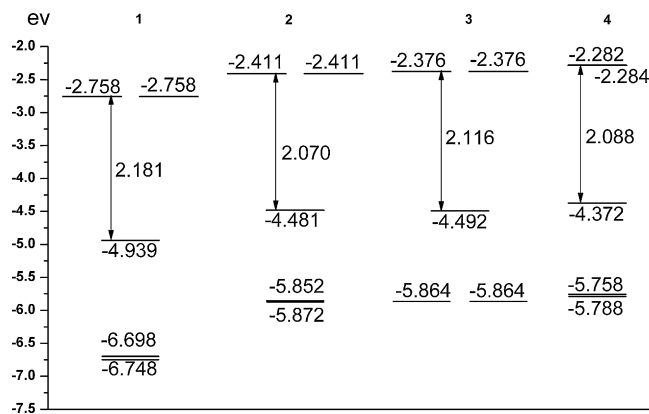


Fig. 3. The orbital energies from HOMO-2 to LUMO+1 of ZnPc (**1**), Zn[Pc( $\alpha$ -OC<sub>5</sub>H<sub>11</sub>)<sub>4</sub>] (**2**), Ni[Pc( $\alpha$ -OC<sub>5</sub>H<sub>11</sub>)<sub>4</sub>] (**3**), and Zn[Pc( $\alpha$ -OC<sub>5</sub>H<sub>11</sub>)<sub>4</sub>]-H<sub>2</sub>O (**4**).

crystal [42]. In other words, forming the novel dimeric supramolecular structure {Zn[Pc( $\alpha$ -OC<sub>5</sub>H<sub>11</sub>)<sub>4</sub>]-H<sub>2</sub>O}<sub>2</sub> from two molecules of 1,8,15,22-tetrakis(3-pentyloxy)phthalocyaninato zinc complex requires bulky non-peripheral substituents, which induces the non-planarity of the phthalocyaninato zinc molecule and therefore ensures the five coordination of the zinc ion rather than traditional six coordination. Further research about the effect of the non-planarity on the coordination of zinc ion by synchronously introducing two coordinating water molecules above and below the phthalocyaninato zinc plane and changing the 3-pentyloxy group to a smaller substituent is in progress.

### 3.2. Molecular orbitals

The energy levels of the molecular orbitals from HOMO-2 to LUMO+1 of **1–4** are shown in Fig. 3. Fig. 4 shows the orbital maps of HOMO and LUMO of **4**. Figs. S1–S4 (Supplementary Data) depict the maps of the main orbitals involved in the electronic transitions in the electronic absorption spectra of **1–4**, respectively. The introduction of the four electron-donating alkoxy groups in **2** lifts the energy levels of both HOMO and LUMO of **1** from -4.94 to -4.48 and -2.76 eV to -2.41 eV, respectively. Due to the more significant increase in the energy of HOMO than that of LUMO, the energy gap from HOMO to LUMO exhibits some decrease from 2.18 eV for **1** to 2.07 eV for **2**, indicating that the Q band of **2** should appear red shifted from that of **1**.

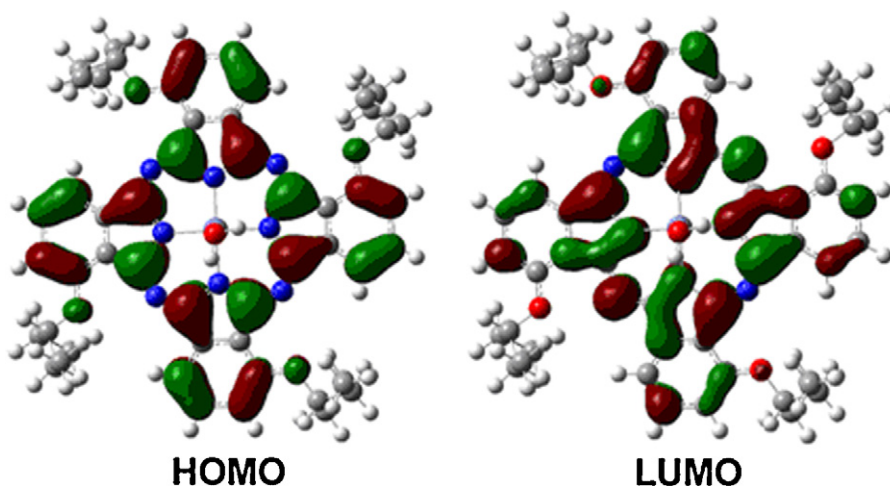


Fig. 4. Molecular orbital maps of the HOMO and LUMO of Zn[Pc( $\alpha$ -OC<sub>5</sub>H<sub>11</sub>)<sub>4</sub>]-H<sub>2</sub>O (**4**).



**Table 3**

Calculated atomic charge distribution (in e) with NBO method for ZnPc (**1**), Zn[Pc( $\alpha$ -OC<sub>5</sub>H<sub>11</sub>)<sub>4</sub>] (**2**), Ni[Pc( $\alpha$ -OC<sub>5</sub>H<sub>11</sub>)<sub>4</sub>] (**3**), and Zn[Pc( $\alpha$ -OC<sub>5</sub>H<sub>11</sub>)<sub>4</sub>]-H<sub>2</sub>O (**4**).

Atom <sup>a</sup>	<b>1</b>	<b>2</b>	<b>3</b>	<b>4<sup>b</sup></b>
M	1.663	1.658	0.937	1.683
N <sub>1</sub>	−0.759	−0.765	−0.604	−0.751
C <sub>α1</sub>	0.440	0.440	0.439	0.441
C <sub>α2</sub>	0.440	0.435	0.435	0.440
C <sub>β1</sub>	−0.083	−0.131	−0.128	−0.128
C <sub>β2</sub>	−0.083	−0.068	−0.066	−0.069
C <sub>γ1</sub>	−0.195	0.371	0.370	0.368
C <sub>γ2</sub>	−0.195	−0.225	−0.224	−0.227
C <sub>δ1</sub>	−0.230	−0.320	−0.319	−0.318
C <sub>δ2</sub>	−0.230	−0.212	−0.208	−0.211
N <sub>2</sub>	−0.498	−0.486	−0.477	−0.493
H <sub>α2</sub>	0.250	0.251	0.251	0.250
H <sub>β1</sub>	0.240	0.237	0.237	0.235
H <sub>β2</sub>	0.240	0.238	0.237	0.236
O		−0.526	−0.525	−0.528
C <sub>1</sub>		0.098	0.098	0.098
C <sub>2</sub>		−0.471	−0.479	−0.471
C <sub>3</sub>		−0.677	−0.682	−0.675
C <sub>4</sub>		−0.480	−0.471	−0.480
C <sub>5</sub>		−0.682	−0.676	−0.682

<sup>a</sup> See Fig. 1 for atomic labeling.

<sup>b</sup> The charges for **4** are from isoindazole ring **I**.

Upon nickel substitution of the central zinc of **2**, the energy level of HOMO decreases to −4.49 eV for **3**, while the energy level of LUMO increases to −2.38 eV, resulting in the increased HOMO–LUMO energy gap from 2.07 eV for **2** to 2.12 eV for **3**. These results indicate that substituting the central metal with one that has a smaller radius decreases both the oxidizability and reductibility of phthalocyaninato metal complex and therefore increases its stability. However, the influence of the central metal substitution on the molecular orbitals is much weaker than that of the non-peripheral substitution. As can be seen, the alkoxy groups in **2** lift both the HOMO and LUMO of **1** by as much as 0.46 eV, whereas changing zinc to nickel only shifts the frontier orbital by less than 0.04 eV.

The introduction of a water molecule on the axial position of **2** further increases the energy levels of both HOMO and LUMO, to −4.37 and −2.28 eV, respectively. Similar to the central metal substitution, the influence of axial substitution on the frontier molecular orbital is much weaker than that of the non-peripheral substitution, though the introduced water molecule destroys the C<sub>4</sub> symmetry of **2** and, thus, causes the loss of degeneracy between LUMO and LUMO+1.

The influence of the non-peripheral substitution, central metal, and axial substitution on the molecular orbital energy level can be well rationalized by analyzing the orbital distribution. As can be seen from Fig. 4 and S1–S4 (Supplementary Data), there is some orbital component in the oxygen atoms of the alkoxy substituents in the HOMO of **4** in addition to being mainly distributed on the carbon atoms of the phthalocyanine ring. It is also true for the LUMO. As a result, the non-peripheral substituents show obvious effects on the orbital energies of both HOMO and LUMO. Due to the greater distribution from the oxygen atoms of the alkoxy substituents in the HOMO than in the LUMO, the HOMO energy increases more than the LUMO energy. However, there is almost no orbital contribution from the central metal and the axial coordinated water for the HOMO and LUMO, which explains the very slight effect of the central metal and the axial substitution on the molecular orbital energy.

### 3.3. Atomic charge

Table 3 lists the atomic charge (in e) of the skeleton atoms for **1–4** calculated by the NBO population method. As can be seen, the negative charge on the C<sub>γ1</sub> atom of **1** changed to a positive

charge with the value of 0.371 e due to its direct connection to the electronegative oxygen atom when the electron-donating 3-pentyloxy group is attached onto it in **2**. Along with the charge conversion from negative to positive on the C<sub>γ1</sub> atom in **2**, the negative charge on atoms directly connected with the C<sub>γ1</sub> atom increases from −0.083 and −0.230 e in **1** to −0.131 and −0.320 e in **2** for the C<sub>β1</sub> and C<sub>δ1</sub> atoms, respectively. Contrary to the C<sub>β1</sub> and C<sub>δ1</sub> atoms, the negative charge on both the C<sub>β2</sub> and C<sub>δ2</sub> atoms decreases upon the 3-pentyloxy substitution, while the negative charge distributed on the C<sub>γ2</sub> atom increases. Associated with the increase of the Zn–N<sub>1</sub> bond length from **1** to **2**, the positive charge on zinc decreases slightly from 1.663 to 1.658 e, while the negative charge on the isoindole nitrogen atoms increases from −0.759 to −0.765 e.

Substituting the central zinc of **2** with nickel decreases the positive charge on the central metal, from 1.658 e for **2** to 0.937 e for **3**. With the decrease of M–N<sub>1</sub> bond length from **2** to **3**, the negative charge on the isoindole nitrogen atom in **3** decreases significantly by 0.161 e in comparison with that in **2**. In addition, both the positive charge on C<sub>α1</sub>, C<sub>α2</sub>, and C<sub>γ1</sub> and the negative charge on the nitrogen atoms and other carbon atoms of the phthalocyanine ligand of **3** also show some decrease. However, except for the central metal and isoindole nitrogen atoms, the difference in the charge distribution on other atoms between **2** and **3** is negligible. These results indicate that the influence of the central metal substitution on the charge distribution of the phthalocyaninato metal complexes is limited mainly to the atoms directly connected with the central metal.

The water molecule in the axial position makes the positive charge on the zinc atom increase to 1.683 e in **4**. The water molecule shows a net charge of 0.033 e, revealing that the partial lone pair electron of the oxygen atom of the water molecule transfers to the unoccupied orbital of the zinc cation, which indicates the strong interaction between oxygen and zinc. Associated with the increase of the Zn–N<sub>1</sub> bond length and the non-planarity, the negative charge on the isoindole nitrogen atoms in **4** shows some decrease in comparison with that in **2**. However, there is no significant difference between the charge distributions on the other atoms of the phthalocyanine ligand, which indicates that the influence of the axial coordination on the charge distribution of the phthalocyaninato metal complexes is also limited mainly to the atoms directly connected with the central metal.

### 3.4. Infrared spectra

The calculated infrared (IR) spectra of **1–4** are shown in Fig. 5. As can be seen, the simulated IR spectrum of **1** showed the typical peaks of the phthalocyaninato metal complexes. The two peaks at 3096 and 3080 cm<sup>−1</sup> are both due to the asymmetric C–H stretching vibrations on the benzene ring according to our calculation. The peaks in the region of 1600–900 cm<sup>−1</sup> are all vibration modes of the isoindole deformation (mainly C–C stretching). The most intense peak in this region of **1** appears at 1104 cm<sup>−1</sup>, which is due to the vibration of C–H rocking and C–N stretching in the plane of the benzene ring. The second strongest peak appears at 1327 cm<sup>−1</sup> with the same vibration mode. The peak appearing at 719 cm<sup>−1</sup> among the peaks below 900 cm<sup>−1</sup> is attributed to the symmetric out of plane bending vibration of the isoindole.

The wavenumber of the vibration modes increases with the introduction of the 3-pentyloxy side chains from **1** to **2**, and the most noticeable difference appears in the region of 2800–3200 cm<sup>−1</sup>. Besides the two peaks at 3080 and 3096 cm<sup>−1</sup> due to the C–H stretching of the benzene rings, a couple of new peaks appear in the spectrum of **2** in the region from 2911 to 3080 cm<sup>−1</sup>, which are clearly due to the symmetrical and asymmetrical C–H stretching modes of the 3-pentyloxy groups according to our cal-

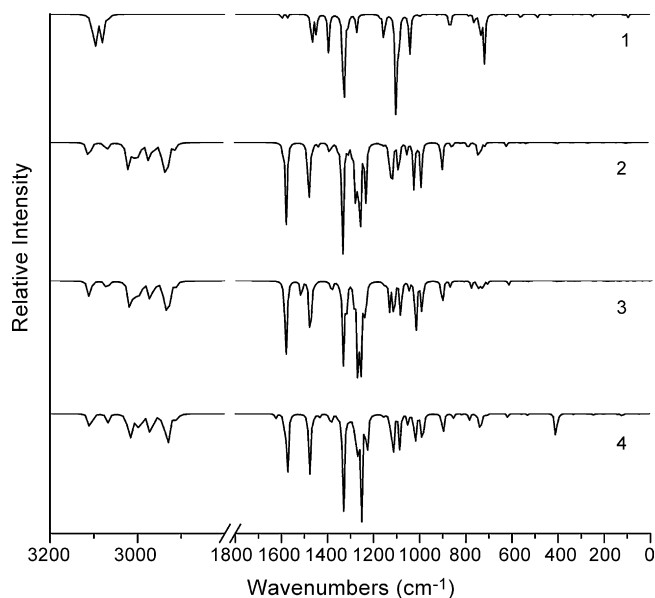


Fig. 5. Simulated IR spectra of ZnPc (**1**), Zn[Pc( $\alpha$ -OC<sub>5</sub>H<sub>11</sub>)<sub>4</sub>] (**2**), Ni[Pc( $\alpha$ -OC<sub>5</sub>H<sub>11</sub>)<sub>4</sub>] (**3**), and Zn[Pc( $\alpha$ -OC<sub>5</sub>H<sub>11</sub>)<sub>4</sub>]·H<sub>2</sub>O (**4**).

culation. The peaks at 1600–900 cm<sup>−1</sup> of **2** are mainly due to the isonidole deformation together with some contribution from the C–H bending vibration of the substituent, which are not included in **1**. The most intense absorption of **2** appears at 1327 cm<sup>−1</sup>, corresponding to the second strongest peak of **1** at 1327 cm<sup>−1</sup> with the same vibration mode. In the region below 800 cm<sup>−1</sup>, the strong peak of **1** at 719 cm<sup>−1</sup> due to the symmetric isonidole out of plane bending shifts to 742 cm<sup>−1</sup> in **2**. Meanwhile, a new peak due to the vibration of the ring in plane deformation appears at 619 cm<sup>−1</sup>.

Fig. 5 shows that the IR spectra of **2** and **3** are very similar for most peaks, and only a few shifts in the wavenumber are found. The peaks of **2** at 1573, 1473, 1327, and 1250 cm<sup>−1</sup> shifts to 1581, 1481, 1334, and 1258 cm<sup>−1</sup> in **3**, respectively. The fact that the peaks of **3** are blue shifted with respect to corresponding peaks of **2** for these vibrations is in line with the results revealed in the Molecular Structure section. That is, the central metal with small radius shortened some bond lengths of the phthalocyanine macrocycle. In addition, the peak of **2** at 742 cm<sup>−1</sup> shifts to 735 cm<sup>−1</sup> in **3**, showing some red shift. Interestingly, there is a weak peak at 1519 cm<sup>−1</sup> for **3** attributed to the C $\alpha$ –N<sub>2</sub> stretching vibration, which is not found in the spectrum of **2**. The probable reason for this is that this vibration in **2** has shifted to the red side of 1519 cm<sup>−1</sup> due to a longer C $\alpha$ –N<sub>2</sub> bond than that in **3** and, therefore, has been covered up by the strong vibration at 1743 cm<sup>−1</sup>.

Comparing the IR spectrum of **4** with that of **2** shows that, except for the vibration modes of the water molecule and Zn–O bond, the IR spectra of **2** and **4** are very similar to each other when shifts in wavenumber are ignored. As shown in Fig. 5, almost all of the peaks of **4** from 500 to 3200 cm<sup>−1</sup> have counterparts with the same vibrations in the spectrum of **2**, which is in line with the very small difference in the structural parameter between **4** and **2** revealed in the Molecular Structure section. The peaks in the IR spectrum of **4** are red shifted with respect to those of **2**, also corresponding to the molecular structure result. The most obvious difference between **4** and **2** is the new peak at 411 cm<sup>−1</sup> for **4**, which does not exist in the spectrum of **2**. This peak is assigned to the bending vibration of the water molecule relative to the mean phthalocyanine plane. The weak peak of **4** at 1624 cm<sup>−1</sup> is due to the O–H bending vibration and thus also does not appear in the spectrum of **2**.

To validate the calculated results, the calculated and experimental IR spectra of **4** are compared in Fig. 6. As shown in the figure, the

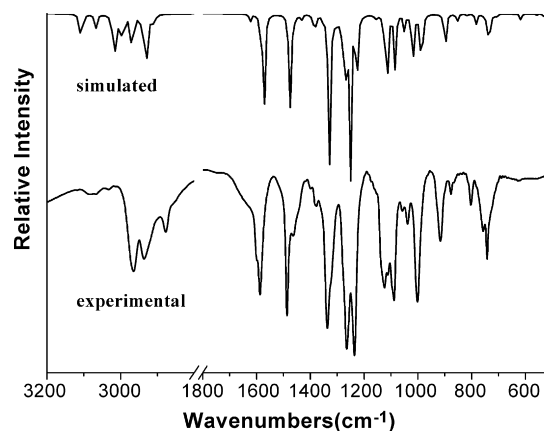


Fig. 6. Comparison of the simulated and experimental IR spectra of Zn[Pc( $\alpha$ -OC<sub>5</sub>H<sub>11</sub>)<sub>4</sub>]·H<sub>2</sub>O (**4**).

simulated IR spectrum of **4** corresponds well with the recorded one. Fig. 7 gives the intuitive correspondence relationship of the calculated and experimental results by fitting them to a linear function. The slope of the line is 0.9993 and the intercept is 3.66 cm<sup>−1</sup>, which shows a good agreement between the calculated and experimental data.

### 3.5. Electronic absorption spectra

Fig. 8 shows the simulated electronic absorption spectra of the four phthalocyaninato metal complexes **1–4**, and Table 4 organizes the main peaks, their corresponding oscillator strength, and the nature of the electronic transitions. Molecule **1** has a couple of Soret bands before 400 nm and one Q band at 595 nm, which corresponds well with the calculated result at PBE0/SVP level appearing at 576 nm [18]. The calculation results reveal that the Q band is mainly due to the electron transition from HOMO to LUMO and, thus, should correspond with the energy gap of HOMO–LUMO. However, the couples of Soret bands, which are due to the electron transitions from the low-lying occupied orbitals to the degenerate LUMO orbitals, are much more complicated than the Q bands. It is worth noting that because of the planar structure of **1**, the weak peak at 472 nm for non-planar PbPc, which is due to the electron transition from HOMO–1 to LUMO, disappears in the electronic absorption spectrum of **1** [25].

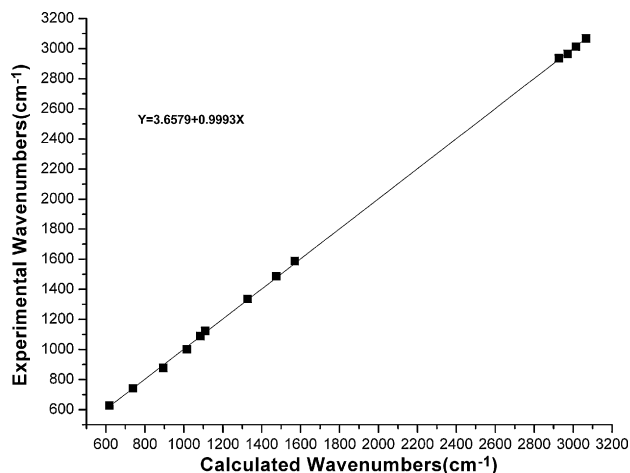
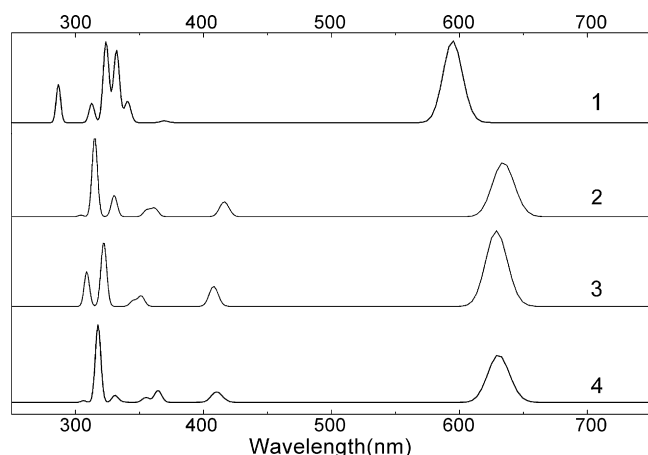


Fig. 7. Consistency of the wavenumbers of the main peaks in the calculated and experimental IR spectra of Zn[Pc( $\alpha$ -OC<sub>5</sub>H<sub>11</sub>)<sub>4</sub>]·H<sub>2</sub>O (**4**).



**Fig. 8.** Simulated electronic absorption spectra of ZnPc (**1**), Zn[Pc( $\alpha$ -OC<sub>5</sub>H<sub>11</sub>)<sub>4</sub>] (**2**), Ni[Pc( $\alpha$ -OC<sub>5</sub>H<sub>11</sub>)<sub>4</sub>] (**3**), and Zn[Pc( $\alpha$ -OC<sub>5</sub>H<sub>11</sub>)<sub>4</sub>]-H<sub>2</sub>O (**4**).

When four 3-pentyloxy groups are introduced into the non-peripheral positions of **1**, the Q band is found to shift from 595 nm for **1** to 634 nm for **2**, in line with the decreased HOMO–LUMO energy gap from **1** to **2**, which was mentioned in the Molecular Orbital section. Meanwhile, the Soret bands of **2** also show some red shift in comparison with those of **1** because the energies of other low-lying occupied orbitals increase more than that of LUMO, as shown in Fig. 8 and Table 4. Nevertheless, a new band appears in the spectrum of **2** at 416 nm, which is mainly due to the electron transition from HOMO-1 to LUMO. This band is very common for alkoxy-substituted phthalocyaninato compounds and is usually attributed to the  $n-\pi^*$  transition [25]. The existence of similar bands in the spectra of **3** and **4** further supports this assignment.

The electronic absorption spectra of **2** and **3** are very similar, and there is only a small shift in the wavelength. The Q band of **2** at 634 nm shifts to 629 nm for **3** due to the central metal substitution, in line with the trend found for the HOMO–LUMO energy gaps. Similarly, the Soret bands before 400 nm are all found to be slightly blue shifted from **2** to **3**. It is also true for the band of **2** at 416 nm, which is due to the weak  $n-\pi^*$  transition. However, the nature of this band for **3** changes to the electron transition from HOMO-3 to LUMO. The orbital maps shown in Fig. S1–S4 (Supplementary Data)

**Table 4**

Calculated wavelength ( $\lambda$ /nm), oscillator strength ( $f$ ), and electron transition nature in the electronic absorption spectra of ZnPc (**1**), Zn[Pc( $\alpha$ -OC<sub>5</sub>H<sub>11</sub>)<sub>4</sub>] (**2**), Ni[Pc( $\alpha$ -OC<sub>5</sub>H<sub>11</sub>)<sub>4</sub>] (**3**), and Zn[Pc( $\alpha$ -OC<sub>5</sub>H<sub>11</sub>)<sub>4</sub>]-H<sub>2</sub>O (**4**).

	$\lambda$ /nm	$f$	Electronic transition nature [H = HOMO, L = LUMO]	
<b>1</b>	594.6	0.4196	H-0 → L+1(+72%)	H-4 → L+0(+11%)
	340.7	0.1090	H-8 → L+1(+54%)	H-4 → L+1(+31%)
	323.8	0.4157	H-4 → L+1(+36%)	H-8 → L+1(28%)
	286.6	0.1949	H-13 → L+0(+79%)	
<b>2</b>	634.1	0.4690	H-0 → L+0(+72%)	H-5 → L+1(+7%)
	416.2	0.1284	H-1 → L+0(+77%)	H-1 → L+1(+18%)
	355.6	0.0581	H-6 → L+0(+49%)	H-4 → L+1(14%)
	330.2	0.1832	H-10 → L+1(+66%)	H-10 → L+0(+12%)
	315.0	0.6883	H-5 → L+0(+21%)	H-4 → L+1(+21%)
<b>3</b>	628.8	0.4418	H-0 → L+0(+55%)	H-0 → L+1(21%)
	407.9	0.1169	H-3 → L+0(85%)	H-3 → L+1(10%)
	351.3	0.0608	H-6 → L+0(69%)	H-7 → L+1(+15%)
	322.0	0.3776	H-7 → L+0(+36%)	H-11 → L+0(+27%)
	308.8	0.2030	H-11 → L+0(33%)	H-0 → L+6(21%)
<b>4</b>	630.6	0.4607	H-0 → L+0(+74%)	H-4 → L+1(+9%)
	630.3	0.4589	H-0 → L+1(+74%)	H-4 → L+0(9%)
	411.1	0.1003	H-1 → L+1(+71%)	H-1 → L+0(15%)
	364.5	0.1151	H-5 → L+1(+33%)	H-4 → L+0(27%)
	364.4	0.1155	H-5 → L+0(+31%)	H-4 → L+1(+27%)
	317.6	0.7497	H-4 → L+0(+39%)	H-5 → L+1(+26%)

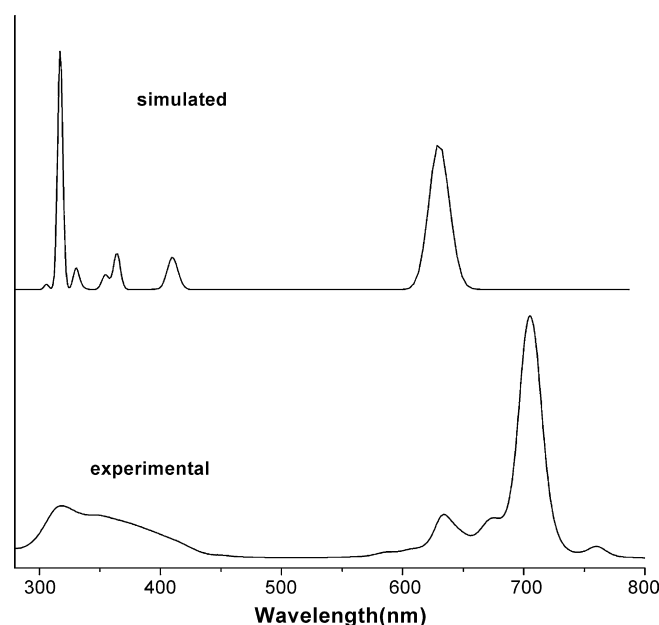


**Fig. 9.** Comparison of the simulated and experimental electronic absorption spectra of Zn[Pc( $\alpha$ -OC<sub>5</sub>H<sub>11</sub>)<sub>4</sub>]-H<sub>2</sub>O (**4**).

revealed that the HOMO-1 orbital of **2** has the same composition as the HOMO-3 orbital of **3**. Consequently, the two bands at 416 nm for **2** and 408 nm for **3** can be considered as having the same electron transition nature.

With the decrease of the molecular symmetry from **2** to **4**, the degeneracy of LUMO and LUMO+1 disappears. As the result, the Q band of **2** splits to two bands in **4**, which are at 630 and 631 nm, respectively. Both of the two Q bands of **4** are blue shifted with respect to the Q band of **2**, in line with the orbital energy gaps between HOMO and LUMO or LUMO+1 for **2** and **4**. The weak  $n-\pi^*$  transition band of **2** at 416 nm also shows some blue shift in the electronic absorption spectrum of **4**, to 411 nm, which is mainly due to electron transition from HOMO-1 to LUMO+1 coupled with the electron transition from HOMO-1 to LUMO.

The calculated and experimental electronic absorption spectra of **4** are compared in Fig. 9. Corresponding to the calculated Q bands



at 630 and 631 nm, only one strong Q band is recorded experimentally at 705 nm. However, the observed vibration band around 640 nm and the two weak bands at the two sides of the Q band in the experimental electronic absorption spectrum of **4** do not have counterparts in the simulated electronic absorption spectrum. The probable reason is that our calculation was conducted in a vacuum, which cannot reproduce bands due to vibration and conglomeration in solution as in the experimental case. On the contrary, the calculation results predict several well-separated Soret bands, which cannot be separated in the experimental spectra and take a broad envelope of overlapping bands in the 250–400 nm region due to the weak intensity. Nevertheless, the experimentally observed Soret band at 324 nm corresponds well with the calculated one at 318 nm. As a whole, the simulated electronic absorption spectrum of **4** qualitatively reproduces the characteristic bands in both the Soret and Q band region, indicating the good capability of the TDDFT method to calculate electronic absorption spectra.

#### 4. Conclusions

In summary, we investigated the molecular structure, molecular orbitals, atomic charge, IR spectra, and electronic absorption spectra of ZnPc and its non-peripheral alkoxy substituted, central metal substituted, and axial coordinated derivatives by DFT and TDDFT calculations. The substitution of bulky 3-pentyloxy groups at the non-peripheral positions of the phthalocyanine ring was revealed to deflect the isoindole units in the direction that the isoindole units extend, lift the frontier molecular orbitals, change the atomic charge distribution and shift the bands of IR and electronic absorptions. However, the effect of the central metal substitution on the electronic structure and spectroscopic properties of the phthalocyanine complex is very limited. Axial coordination significantly increases the non-planarity of the phthalocyanine ring and, thus, alters the electronic structure and properties of the phthalocyaninato zinc complex, which leads to the formation of the novel dimeric supramolecular structure by intermolecular hydrogen bonds instead of forming a one-dimensional chain.

#### Acknowledgments

Financial support from the Natural Science Foundation of China (Grant No. 20931001), Beijing Municipal Commission of Education, China Postdoctoral Science Foundation (20090460210), and University of Science and Technology Beijing is gratefully acknowledged. We are also grateful to the Shandong Province High Performance Computing Center for a grant of computer time.

#### Appendix A. Supplementary data

Supplementary data associated with this article can be found, in the online version, at [doi:10.1016/j.jmgs.2010.03.004](https://doi.org/10.1016/j.jmgs.2010.03.004).

#### References

- [1] N.B. McKeown, *Phthalocyanine Materials: Synthesis, Structure and Function*, Cambridge University Press, Cambridge, UK, 1998.
- [2] A.B.P. Lever, C.C. Leznoff, *Phthalocyanine: Properties and Applications*, VCH, New York, 1989–1996.
- [3] K.M. Kadish, K.M. Smith, R. Guilard, *The Porphyrin Handbook*, Academic Press, San Diego, CA, 2000–2003.
- [4] P. Gregory, *High-technology Applications of Organic Colorants*, Plenum Press, New York, 1989–1991.
- [5] P.J. Gregory, *Industrial applications of phthalocyanines*, *J. Porphyrins Phthalocyanines* 4 (2000) 432–437.
- [6] R. Ao, L. Kilmert, D. Haarer, *Present limits of data storage using dye molecules in solid matrices*, *Adv. Mater.* 7 (1995) 495–499.
- [7] D. Birkett, *Creating an information revolution*, *Chem. Ind.* 5 (2000) 178–181.
- [8] F.H. Moser, A.L. Thomas, *Manufacture and applications The Phthalocyanines*, vols. 1 and 2, CRC Press, Boca Raton, FL, 1983.
- [9] D. Wöhrl, D. Meissner, *Organic solar cells*, *Adv. Mater.* 3 (1991) 129–138.
- [10] H. Eichhorn, *Mesomorphic phthalocyanines, tetraazaporphyrins, porphyrins and triphenylenes as charge-transporting materials*, *J. Porphyrins Phthalocyanines* 4 (2000) 88–102.
- [11] J.D. Wright, *Gas adsorption on phthalocyanines and its effect on electrical properties*, *Prog. Surf. Sci.* 31 (1989) 1–60.
- [12] A.W. Snow, W.R. Barger, *Properties and applications*, in: C.C. Leznoff, A.B.P. Lever (Eds.), *Phthalocyanines*, VCH, New York, 1989, pp. 341–392.
- [13] H. Nalwa, S.J.S. Shirk, *Properties and applications*, in: C.C. Leznoff, A.B.P. Lever (Eds.), *Phthalocyanines*, VCH, New York, 1996, pp. 79–182.
- [14] J.S. Shirk, R.G.S. Pong, S.R. Flom, H. Heckmann, M. Hanack, *Effect of axial substitution on the optical limiting properties of indium phthalocyanines*, *J. Phys. Chem. A* 104 (2000) 1438–1449.
- [15] G.D.L. Torre, P. Vázquez, F. Agulló-Pérez, T. Torres, *Phthalocyanines and related compounds: organic targets for nonlinear optical applications*, *J. Mater. Chem.* 8 (1998) 1671–1683.
- [16] E.A. Lukanets, *Phthalocyanines as photosensitizers in the photodynamic therapy of cancer*, *J. Porphyrins Phthalocyanines* 3 (1999) 424–432.
- [17] A. Hasrat, J.E.V. Lier, *Metal complexes as photo- and radiosensitizers*, *Chem. Rev.* 99 (1999) 2379–2450.
- [18] A.D. Quartarolo, I. Lanzo, E. Sicilia, N. Russo, *Can phthalocyanines and their substituted a-para-(methoxy)phenyl derivatives act as photosensitizers in photodynamic therapy? A TD-DFT study*, *Phys. Chem. Chem. Phys.* 11 (2009) 4586–4592.
- [19] B. Cosomelli, G. Roncucci, D. Dei, L. Fantetti, F. Ferroni, M. Ricci, D. Spinelli, *Synthesis and antimicrobial activity of new unsymmetrical substituted zinc phthalocyanines*, *Tetrahedron* 59 (2003) 10025–10030.
- [20] H.I. Beltrán, R. Esquivel, A. Sosa-Sánchez, J.L. Sosa-Sánchez, L.S. Zamudio-Rivera, *Inorg. Chem.* 43 (2004) 3555–3557.
- [21] C.H. Langford, B.R. Hollebone, T. Vandernoot, *Photoelectrochemistry and spectroscopy of metal phthalocyanine films on a transparent semiconducting electrode*, *Adv. Chem. Ser.* 8 (1980) 139–154.
- [22] E.H.G. Langner, W.L. Davis, R.F. Shago, J.C. Swarts, *Spectroscopic and liquid crystal properties of phthalocyanine macromolecules with biomedical applications*, in: G.R. Newkome, I. Manner, U.S. Schubert (Eds.), *Metal-containing and Metallo-supramolecular Polymers and Materials*, Am. Chem. Soc. Press, New York, 2006, pp. 443–456 (Chapter 31).
- [23] P.C. Lo, C.M.H. Chan, J.Y. Liu, W.P. Fong, D.K.P. Ng, *Highly photocytotoxic glucosylated silicon(IV) phthalocyanines. Effects of peripheral chloro substitution on the photophysical and photodynamic properties*, *J. Med. Chem.* 5 (2007) 2100–2107.
- [24] Y.X. Zhang, X. Cai, X.X. Zhang, H. Xu, Z.Q. Liu, J.J. Jiang, *Time-dependent density functional theory studies of the electronic absorption spectra of metallophthalocyanines of group IVA*, *Int. J. Quant. Chem.* 107 (2007) 952–961.
- [25] Y.X. Zhang, X.X. Zhang, Z.Q. Liu, Y.Z. Bian, J.J. Jiang, *Structures and properties of 1,8,15,22-tetrasubstituted phthalocyaninato-lead complexes: the substitutional effect study based on density functional theory calculations*, *J. Phys. Chem. A* 109 (2005) 6363–6370.
- [26] X. Cai, Y.X. Zhang, X.X. Zhang, J.J. Jiang, *Structures and properties of 2,3,9,10,16,17,23,24-octasubstituted phthalocyaninato-lead complexes: the substitutional effect study on the basis of density functional theory calculations*, *J. Mol. Struct.: TheoChem.* 801 (2006) 71–80.
- [27] A. Rosa, G. Ricciardi, *The optical spectra of NiPc, NiPz, NiTBP, and NiPc: electronic effects of meso-tetraaza substitution and tetrabenzo annulation*, *J. Phys. Chem. A* 105 (2001) 3311–3327.
- [28] N. Marom, L. Kronik, *Density functional theory of transition metal phthalocyanines. I: electronic structure of NiPc and CoPc—self-interaction effects*, *Appl. Phys. A* 95 (2009) 159–163.
- [29] T. Strenalyuk, S. Samdal, H.V. Volden, *Molecular structures of phthalocyaninato-zinc and hexadecafluorophthalocyaninato-zinc studied by gas-phase electron diffraction and quantum chemical calculations*, *J. Phys. Chem. A* 111 (2007) 12011–12018.
- [30] G. Ricciardi, A. Rosa, *Ground and excited states of zinc phthalocyanine studied by density functional methods*, *J. Phys. Chem. A* 105 (2001) 5242–5254.
- [31] Z.Q. Liu, X.X. Zhang, Y.X. Zhang, J.J. Jiang, *Theoretical investigation of the molecular, electronic structures and vibrational spectra of a series of first transition metal phthalocyanines*, *Spectrochim. Acta A* 67 (2007) 1232–1246.
- [32] R.J. Li, Y.X. Zhang, Y. Zhou, S. Dong, X.Y. Zhang, Y.Z. Bian, J.J. Jiang, *H<sub>2</sub>O-involved hydrogen bonds in pseudo-double-decker supramolecular structure of 1,8,15,22-tetrasubstituted phthalocyaninato zinc complex*, *Cryst. Growth Des.* 8 (2008) 4454–4459.
- [33] A.D. Becke, *Density-functional thermochemistry. III. The role of exact exchange*, *J. Chem. Phys.* 98 (1993) 5648–5652.
- [34] T.H. Dunning Jr., P.J. Hay, in: H.F. Schaefer III (Ed.), *Modern Theoretical Chemistry*, Plenum, New York, 1976.
- [35] P.J. Hay, W.R. Wadt, *Ab initio effective core potentials for molecular calculations. Potentials for the transition metal atoms Sc to Hg*, *J. Chem. Phys.* 82 (1985) 270–283.
- [36] W.R. Wadt, P.J. Hay, *Ab initio effective core potentials for molecular calculations. Potentials for main group elements Na to Bi*, *J. Chem. Phys.* 82 (1985) 284–298.
- [37] P.J. Hay, W.R. Wadt, *Ab initio effective core potentials for molecular calculations. Potentials for K to Au including the outermost core orbitals*, *J. Chem. Phys.* 82 (1985) 299–310.

- [38] C. Peng, P.Y. Ayala, H.B. Schlegel, M.J. Frisch, Using redundant internal coordinates to optimize equilibrium geometries and transition states, *J. Comput. Chem.* 17 (1996) 49–56.
- [39] NIST Computational Chemistry Comparison and Benchmark Database, NIST Standard Reference Database Number 101, In: D.J. Russell, III (Ed.), 2004. <http://srdata.nist.gov/cccbdb>.
- [40] A.E. Reed, L.A. Curtiss, F. Weinhold, Intermolecular interactions from a natural bond orbital, donor-acceptor viewpoint, *Chem. Rev.* 88 (1988) 899–926.
- [41] M.J. Frisch, G.W. Trucks, H.B. Schlegel, G.E. Scuseria, M.A. Robb, J.R. Cheeseman, J.A. Montgomery Jr., T. Vreven, K.N. Kudin, J.C. Burant, J.M. Millam, S.S. Iyengar, J. Tomasi, V. Barone, B. Mennucci, M. Cossi, G. Scalmani, N. Rega, G.A. Petersson, H. Nakatsuji, M. Hada, M. Ehara, K. Toyota, R. Fukuda, J. Hasegawa, M. Ishida, T. Nakajima, Y. Honda, O. Kitao, H. Nakai, M. Klene, X. Li, J.E. Knox, H.P. Hratchian, J.B. Cross, C. Adamo, J. Jaramillo, R. Gomperts, R.E. Stratmann, O. Yazyev, A.J. Austin, R. Cammi, C. Pomelli, J.W. Ochterski, P.Y. Ayala, K. Morokuma, G.A. Voth, P. Salvador, J.J. Dannenberg, V.G. Zakrzewski, S. Dapprich, A.D. Daniels, M.C. Strain, O. Farkas, D.K. Malick, A.D. Rabuck, K. Raghavachari, J.B. Foresman, J.V. Ortiz, Q. Cui, A.G. Baboul, S. Clifford, J. Cioslowski, B.B. Stefanov, G. Liu, A. Liashenko, P. Piskorz, I. Komaromi, R.L. Martin, D.J. Fox, T. Keith, M.A. Al-Laham, C.Y. Peng, A. Nanayakkara, M. Challacombe, P.M.W. Gill, B. Johnson, W. Chen, M.W. Wong, C. Gonzalez, J.A. Pople, Gaussian 03, Revision B.05, Gaussian, Inc., Pittsburgh, PA, 2003.
- [42] Y.N. Gao, X.M. Zhang, C.Q. Ma, X.Y. Li, J.Z. Jiang, Morphology-controlled self-assembled nanostructures of 5,15-di[4-(5-acetylsulfanyl)pentyl]phenyl porphyrin derivatives. Effect of metal-ligand coordination bonding on tuning the intermolecular interaction, *J. Am. Chem. Soc.* 130 (2008) 17044–17052.